IOP Conf. Series: Materials Science and Engineering **329** (2018) 012016 doi:10.1088/1757-899X/329/1/012016

Comparative microstructural and corrosion development of VCrNiCoFeCu equiatomic multicomponent alloy produced by induction melting and spark plasma sintering

É Fazakas [1,7*)], A Heczel [1,2], D Molnár [3,4], B Varga [5], V. Zadorozhnyy [6], Á Vida [1,2,7]

[1] Bay Zoltán Nonprofit Ltd. for Applied Research, Engineering Division, Budapest, Hungary
[2] Institute of Materials Physics, Eötvös University, Budapest H-1117, Pázmány P. stny 1/A
[3] Materials Science Group, Dalarna University, 791 88 Falun, Sweden
[4] Applied Materials Physics, Department of Materials Science and Engineering, Royal Institute of Technology,Stockholm SE-100 44, Sweden
[5] Transilvania University of Brasov, Bulevardul Eroilor 29, Brașov 500036
[6] National University of Science and Technology «MISIS», Leninsky prosp., 4, Moscow, 119049, Russia
[7]Institute for Solid State Physics and Optics, Wigner Research Centre for Physics, H-1525 Budapest, P.O. Box 49, Hungary

Abstract. The present study focuses on the corrosion behavior of a single-phase FCC high entropy alloy (VCrNiCoFeCu) casted by two different methods: induction melting and spark plasma sintering. The corrosion resistance has been evaluated using immersion tests in 3.5% NaCl solution, the potentiodynamic polarization measurements and the results are compared how is dependent the corrosion rate as a function of the production methods. Our results show that induction melted sample is stable in salty environment. On the other hand, based on the changes of polarization curves, there must be an evolution of oxide films on the SPSed sample until reaching the stable oxide layer.

1. Introduction

Traditional concept of alloy systems has been based on utilizing one or two elements as the principal components, and sometimes, minor quantities of other elements are used to enhance the properties, such as steels, NiAl intermetallics and bulk metallic glasses (BMG) [1]. The main reason is that traditional metallurgical knowledge suggests that complex phases or intermetallics will be easily formed in alloy systems with multiple principal components, and thus lead to poor mechanical properties [2].

In the last decade, the so called High-Entropy Alloys (HEAs) became popular materials because of their unique properties, as high strength and ductility simultaneously [1–3], thermal stability [4–6] and excellent corrosion resistant properties [7–9].

The name comes from the fact that high mixing entropy ΔSmix can dominate the term of Gibbs relation: $\Delta G_{mix} = \Delta H_{mix} - T\Delta S_{mix}$. High entropy comes from the high number of elements in the alloy, since based on the definition as an alloy HEA system is composed of five or more kinds of principal elements in an equimolar or near equimolar ratio, with a small difference in atomic radii (<15%) and concentration of each element is varying from 5 to 35 at%. By this way the significance of the enthalpy of mixing (ΔH_{mix}) is oppressed and the solid solution phase is favoured over the intermetallic phases. This explanation and the name HEA came from Yeh and co-workers from year 2004 [10,11]. With proper composition designing, the HEA exhibits high hardness, excellent ductility as well as promising resistances to wear, oxidation and corrosion [5].

In this paper, we investigate VCrNiCoFeCu high-entropy alloy prepared by induction melting and spark plasma sintering methods. We conducted this comparative analysis for the two methods because the induction melting is not the best for industrial manufacturing due to the diseconomy and limitations in shape and size of final products. By contrast, mechanical alloying (MA) is a more convenient way, which has been widely used for the synthesis of nanocrystalline materials and widens the application scope of HEAs [6,7]. In addition, combined with the novel Spark Plasma Sintering (SPS) technique, bulk metallic glasses and high-entropy alloy can be easily obtained from the as-milled powders [8,9].

2. Experimental procedures

Metal powders of V, Cr, Ni, Co, Fe, Cu with purities of higher than 99.5 wt% and particle size ≤45 μm were used as initial materials. The elemental powders were mixed in equiatomic composition and milled in planetary ball miller (Fritsch pulverisette-4) for 20 h at 400 rpm in an argon atmosphere.

The obtained powder mixtures were sintered under vacuum using an SPS system (FCT System HPD 25). The sintering temperature was measured (0.05K precisely) and controlled by a thermocouple inserted into the graphite die wall at a distance of about 2 mm from the sintered sample. A uniaxial pressuring method was conducted using top and bottom graphite punches. The loading pressure was 90 MPa. A heating rate of 100 K/min was applied from room temperature to 480 °C before slowing down to 20 K/min from 480 °C to 500 °C to avoid temperature overshoot. The sintering temperature ranged from 500 to 550 °C. The holding time at the sintering temperature was in the range 20–30 min. Then the sample was removed from the heated region and a natural cooling was applied so that after about 30 min the specimen was at room temperature. The densified samples had a cylindrical shape, with a diameter of about 10 mm and a thickness of about 4 mm. All characterizations have been realized on these cylinders.

In the case of induction melting, lumps of high purity (99.99%) elements were melted under protecting atmosphere of argon to prepare the VCrNiCoFeCu equi-molar composition alloy.

The Scanning Electron Microscopy (SEM) was taken on FEI Quanta 3D FEG and Zeiss JSM microscopes equipped with Energy Dispersive Spectroscopy (EDS) and also Electron Back Scattered Diffraction (EBSD) instruments of EDAX.

The microstructure was investigated by electron backscatter diffraction (EBSD) using an FEI Quanta 3D scanning electron microscope (SEM). Before the EBSD investigation the surface was mechanically polished with 400, 600, 800, 1200, 2400 grit SiC abrasive. Finally, the surface was polished by 1 μm diamond paste

The chemical composition was examined by energy-dispersive X-ray spectroscopy (EDS) in SEM.

The structure of the alloy was identified by X-ray diffraction with Copper Kα (wavelength, λ=0.15418 nm) radiation in θ-2θ mode scanning from 20^o to 80^o at a scanning rate of 0.5^o/min. For identification of the consistent phases, the PDF database was used. The average lattice parameter was determined by extrapolating the lattice parameters obtained from the different reflections to the diffraction angle of 2Θ= 180° using the Nelson–Riley method [12].

The corrosion resistances of the alloys were evaluated by polarization corrosion method. Potentiostatic polarization curves were measured with 10mV/min scan rate in 3.5% sodium chlorite solution (NaCl) at 25 ^{0}C in three-electrode electrochemical cell using a 20x5 mm polycrystalline Pt wire working electrode and an $Hg/Hg_2Cl_2/KCl$ reference electrode. The Tafel curve measurements were carried out using Zahner potentiostat. Electrochemical characteristic parameters, such as electrochemical corrosion potential (E_{corr}), corrosion current density (j_{corr}), can be obtained by evaluating polarization curves.

3. Results and discussion

3.1. Theory analysis and discussion

In this paper the enthalpy of mixing, atomic-size difference and the parameter Ω for the multi-component VCrNiCoFeCu alloy were calculated using the following equations [13-14]:

$$\Delta H_{mix} = \sum_{i=1, i\neq j}^{n} \Omega_{ij} c_i c_j \quad (1)$$

$$\Delta S_{mix} = -R\sum_{i=1}^{n} c_i Lnc_i \quad (2)$$

where $\Omega_{ij}(=4\Delta H^{mix}_{AB})$ is the regular melt-interaction parameter between *i*th and *j*th elements, c_i and c_j are the i-j atom concentrations, and ΔH^{mix}_{AB} is the mixing enthalpy of binary liquid alloys (the value can be obtained in [10-13]).

$$Delta(\delta) = \sqrt{\sum_{i=1}^{n} c_i (1 - r_i / \bar{r})^2} \quad (3)$$

where n is the number of the components in the alloy system, c_i is the atomic percentage of the *i*th component, $\bar{r}(=\sum_{i=1}^{n} c_i r_i)$ is the average atomic radius, and r_i is the atomic radius which could be obtained from [14-15].

The parameter Ω is defined to predict the solid-solution formation for various multi-component alloys as:

$$\Omega = \frac{T_m \Delta S_{mix}}{|\Delta H_{mix}|} \quad (4)$$

The melting temperature of n-elements alloy, T_m, is calculated using the rule of mixtures:

$$T_m = \sum_{i=1}^{n} c_i (T_m)_i \quad (5)$$

Here, $(T_m)_i$ is the melting point of the i*th* component of alloy. As analyzed above, the value of Ω is positive, and Ω=1 should be proposed as a critical value to form a solid solution. If Ω>1, the contribution of $T\Delta S_{mix}$ will exceed that of ΔH_{mix} for a solid-solution formation. If $\Omega \leq 1$, ΔH_{mix} is the dominant part in the equation, and formation of intermetallic compounds are expected [11].
In the case of VCrNiCoFeCu alloy this value is Ω=15.3.
Considering the small atomic size differences and that the value of Ω is larger than 1 indicates that the strain energy caused by lattice distortion is lower in VCrNiCoFeCu alloy and the entropy effect of ΔS_{mix} is large enough to exceed the ΔH_{mix}. Thus, the component atoms can randomly distribute in the alloy and a simple solid solution is stable [15].

Table 1. Calculated thermodynamic parameters of the VCrNiCoFeCu High Entropy Alloy.

Thermodynamic parameters	**VCrNiCoFeCu**
ρ (g/cm^3)	7.891
ΔH_{mix} (kJ/mol)	-1.7785
ΔG (J/mol)	-28976.76
ΔS_{mix} (J/K·mol)	14.90
T_m (K)	1825.6
Ω	15.30
δ (%) atomic radius	1.938
δ (%) WS radius	2.6654

In Table 1. **ρ** corresponds to density, $\mathbf{\Delta H_{mix}}$ is mixing enthalpy, **ΔG** the Gibbs free energy difference, $\mathbf{\Delta S_{mix}}$ the mixing enthalpy, $\mathbf{T_m}$ is the melting point, **Ω** is the parameter for solid solution formation and **δ** is the atomic size difference calculated in both covalent atomic radii and WS cell radius parameters. Calculating the ΔH_{mix} and δ parameters for a numerous HEA's and metallic glasses, Guo and Liu [14] (see Fig.1 in [14]) could delimitate the following regions in ΔH_{mix} versus δ diagram: HEA with a solid solution phase form when the three parameters are in the range of: $-22 \leq \Delta H_{mix} \leq 7$ kJ/mol, and $\delta < 8.5$ and $\Delta S_{mix} \leq 19.5$ J/(K·mol).

In the case of VCrNiCoFeCu alloy the atomic-size difference δ = 1.938 (in covalent atomic radius) the mixing enthalpy ΔH_{mix}= -1.7785 kJ/mol and ΔS_{mix} = 14.90 J/ (K·mol), respectively, as can be seen Table 1.

The values of Ω and δ for VCrNiCoFeCu match the criteria to form a solid solution.

3.2. Electrochemical properties and variation in the microstructure after the test

The open circuit potential (OCP) and polarization curves with electrochemical characteristic parameters of the investigated alloy in 3.5% sodium chlorite (NaCl) solution are shown in Fig. 1 and 2. The corrosion rates and electrochemical parameters of alloys in 3.5% NaCl solution are presented in Table 2 and 3. The corrosion potentials for induction melted sample are varying from -0.5489 to -0.6539 V_{SCE} and for the SPSed sample from -0.5846 to 0.6921 $V_{SCE,}$ as can be seen in Tables 2 and3.

Corrosion rate obtained from the electrochemical polarization measurements can be calculated by:

$$Corrosion\ \text{rate (mm/y)} = \frac{3.27\times10^{-3}\times j_{corr}\times EW}{\rho} \quad (6)$$

where j_{corr} (in μA/cm^2) is the corrosion current density, EW the equivalent mass of the alloy, and ρ is the density of the alloy. EW is defined as follows [16],

$$EW = \frac{1}{\sum\left(\frac{f_i n_i}{a_i}\right)} \quad (7)$$

where f_i, n_i, and a_i are mass fraction, electrons exchanged, and atomic mass, respectively, of the *i*th alloying element. The EW value of VCrNiCoFeCu is 31.157 and the corrosion rate (mm/y) as a function of the time can be found in Tables 2. and 3.

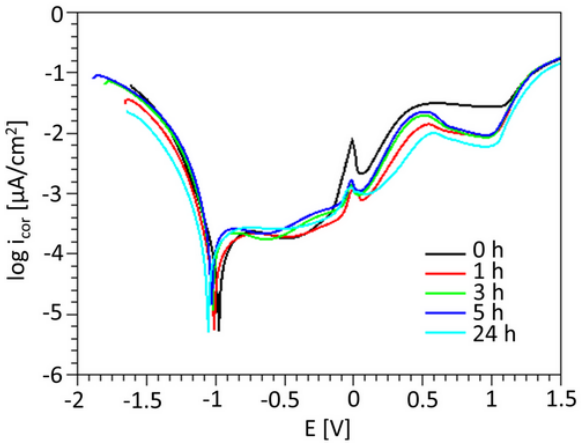

Figure 1. Polarization curves for induction melted VCrNiCoFeCu alloy in 3.5% NaCl solution

Table 2. Electrochemical parameters of the VCrNiCoFeCu alloy, prepared by induction melting method in 3.5% NaCl solution at room temperature (25°C).

Time	E_{corr} (V)	j_{cor} (mA/cm^2)	CR (mm/year)	A (cm^2)
0h	-0.6539	3.2866	0.042044244	0.2
1h	-0.5776	3.5541	0.045466272	
3h	-0.5871	3.2484	0.041555566	
5h	-0.5489	3.2325	0.041352163	
24h	-0.5585	3.3822	0.043267219	

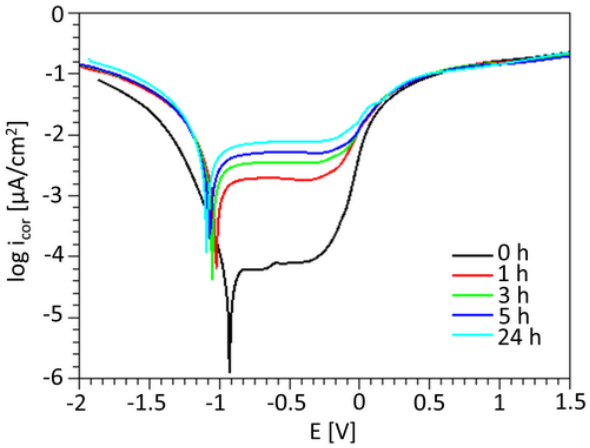

Figure 2. Polarization curves for SPS VCrNiCoFeCu alloy in 3.5% NaCl solution

Table 3. Electrochemical parameters of the VCrNiCoFeCu alloy, prepared by SPS method in 3.5% NaCl solution at room temperature (25°C).

Time	E_{corr} (V)	j_{cor} (mA/cm^2)	CR (mm/year)	A (cm^2)
0h	-0.5846	3.435	0.04394267	0.35
1h	-0.6443	2.5612	0.032764473	
3h	-0.6524	2.2113	0.028288334	
5h	-0.6621	2.1964	0.028097723	
24h	-0.6921	2.1051	0.026929757	

For both alloys three specimens were tested to check the repeatability of the test results. Lower corrosion rate and higher breakdown voltage can be seen in the case of SPSed sample. The transient effect continues until the surface film thins to a degree that it becomes stable with respect to the environment. In the case of induction melted sample corrosion rates were almost stable during 24 h measurements. The differences in chemistry between these two alloys may influence the corrosion performance and this difference is regarded to the preparation methods.
The achieved corrosion resistance of both HEA alloys can be regarded to a protective layer of chromium oxide that has evolved on the surface. In the case of induction-melted sample, this film so thin that it is even not visible by XRD, on the other hand the SEM-EDX demonstrated its presence, as can be seen Figures 5-6.
The pitting corrosion resistance may be quantified using the passive breakdown potential, since sustained breakdown of the passive film is indicative of the onset of pitting corrosion.

This can be seen after the passive regions from which current decreases rapidly with increasing potential. The significantly higher breakdown potential for this HEA designates greater protection against localized corrosion in the chloride-containing solutions, than that of the SS304 [8]. The spikes in current that are seen in Fig. 1. and Fig. 2 may be attributed to metastable pitting. These current fluctuations are caused by corrosion pits, which re-passivize ultimately.

3.3. Microstructure and phase constitution of VCrNiCoFeCu alloys

The XRD results for both alloys are shown on Figures 3-4. The results suggest that both the induction melted and SPS made HEAs are single-phase FCC alloys. It should be mentioned that the in the case of SPS method the sample was polluted by WC (tungsten carbide), which came from the milling jar. The XRD profile of SPS sample in Fig. 4. show significant phase of WC.
The average lattice parameter was determined from the diffraction peak positions using the Nelson-Riley method [18]. The measured X-ray diffractograms indicated both samples have single-phase face-centered cubic (FCC) structure with lattice parameters of a= 0.3612 ± 0.0002 nm and a=0.3665 ± 0.0002, for induction melted and SPSed samples, respectively.

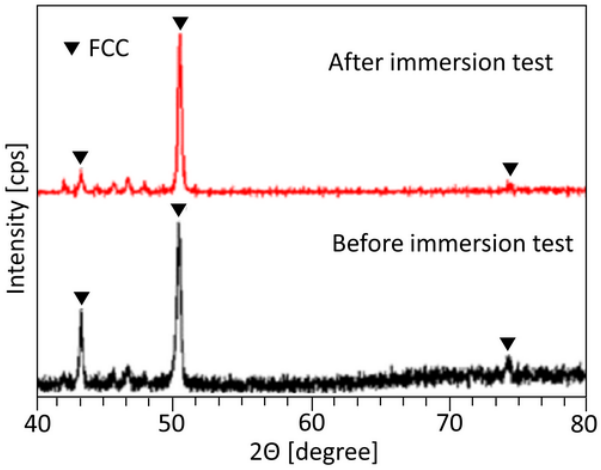

Figure 3. X-ray diffraction patterns of the induction melted VCrNiCoFeCu HEA

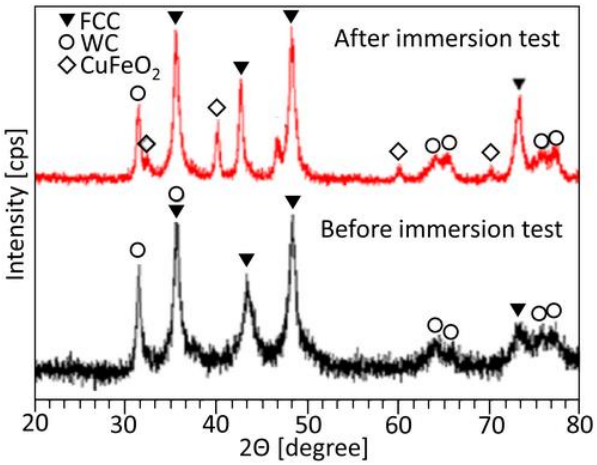

Figure 4. X-ray diffraction patterns of the SPS VCrNiCoFeCu HEA

The SEM micrographs of these alloys are shown in Figures 5-6. Microstructure also plays an important role in corrosion behaviour. Compositional differences which became from the mechanical alloying (the SPS sample was polluted by WC) may result in galvanic coupling, which can be much important than the effect of microstructure on general corrosion.

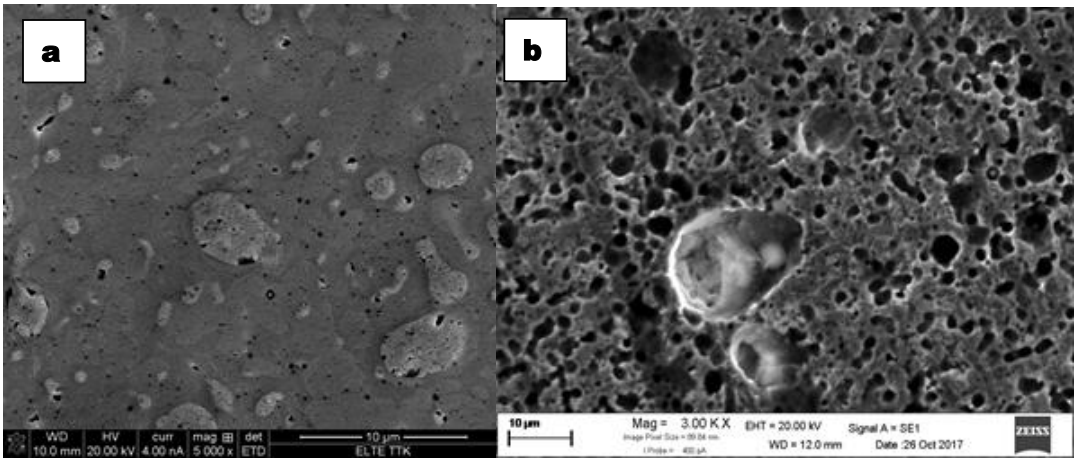

Figure 5. SEM picture of induction melted VCrNiCoFeCu HEA before (a) and after (b) immersion test in 3.5%NaCl solution.

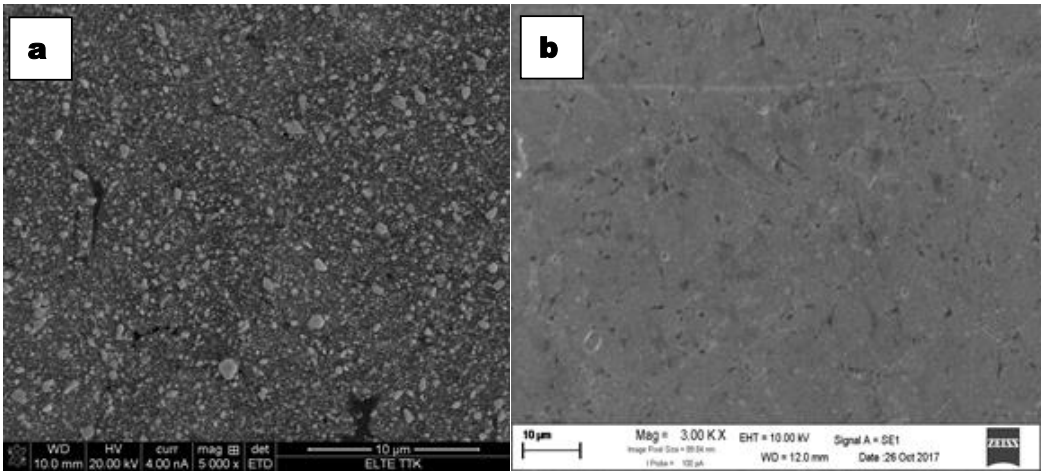

Figure 6. SEM picture of SPS made VCrNiCoFeCu HEA before (a) and after (b) immersion test in 3.5%NaCl solution.

On the SEM figure of induction melted sample (Figure 5.) some chemical inhomogeneity can be seen before the corrosion test. After immersion a thin, high Cr containing film was formed as a protective coating for this alloy. On the Figure 6 one can see the SEM pictures for SPSed sample. The picture of ETD detector shows the surface morphology by secondary electrons. The brighter ones on the picture can be regarded to tungsten carbide pollution (from the milling jar). After the immersion these artefacts are removed, only a layer with high Cr content can be seen with some lower scale pitting corrosion.

4. Conclusions

The two samples of VCrNiCoFeCu prepared by induction melting and spark plasma sintering are crystallized in FCC structure. In the case of induction melted sample, high porosity can be observed. The phenomena can be regarded to Cu segregation effect, and to the fact, that due to their higher viscosity, HEAs tend to have higher porosity than conventional alloys (like steels).

As it can be seen in the Figure 5, a pitting corrosion is observable on the surface after immersion test in 3.5% NaCl solution (for 24 hours). This pitting corrosion behaviour can be attributed to galvanic action between dendrite and inter-dendrite compositions.

In the case of spark plasma sintered alloy, the dendrite like structure is not observable. This can be due to high WC contamination, what is inevitable in the case of mechanical milling.

5. Acknowledgements

This work was supported in part by EIT KIC Raw Materials NoI 15053 "EXTREME" project coordinated by ENEA.

The work was carried out with financial support in part from the Russian Science Foundation, project No. 17-73-20272.

6. References

[1] D V Louzguine-Luzgin, L V Louzguina-Luzgina, T Saito, G Xie, A Inoue 2008 *Structure and properties of high strength and ductile Ti-Fe-Cu-Nb-Sn alloys* Mater. Sci. Eng. A. vol 497 p 126–131 doi:10.1016/j.msea.2008.06.020

[2] B B Sun, M L Sui, Y M Wang, G He, J Eckert, E Ma 2006 *Ultrafine composite microstructure in a bulk Ti alloy for high strength, strain hardening and tensile ductility* Acta Mater vol 54 p 1349–1357 doi:10.1016/j.actamat.2005.11.011

[3] Y Lu, Y Dong, S Guo, L Jiang, H Kang, T Wang, B Wen, Z Wang, J Jie, Z Cao, H Ruan, T Li 2014 *A promising new class of high-temperature alloys: eutectic high-entropy alloys* Sci. Rep vol 4 p 6200 doi:10.1038/srep06200

[4] S Y Chang, M K Chen 2009 *High thermal stability of AlCrTaTiZr nitride film as diffusion barrier for copper metallization* Thin Solid Films vol 517 p 4961–4965 doi:10.1016/j.tsf.2009.03.078

[5] M H Tsai, J W Yeh, J Y Gan 2008 *Diffusion barrier properties of AlMoNbSiTaTiVZr high-entropy alloy layer between copper and silicon* Thin Solid Films vol 516 p 5527–5530 doi:10.1016/j.tsf.2007.07.109

[6] C Ng, S Guo, J Luan, S Shi, C T Liu 2012 *Entropy-driven phase stability and slow diffusion kinetics in an Al 0.5CoCrCuFeNi high entropy alloy* Intermetallics vol 31 p 165–172 doi:10.1016/j.intermet.2012.07.001

[7] É Fazakas, J Q Wang, V Zadorozhnyy, D V Louzguine-Luzgin, L K Varga 2014 *Microstructural evolution and corrosion behavior of $Al_{25}Ti_{25}Ga_{25}Be_{25}$ equi-molar composition alloy* Mater Corros vol 65 doi:10.1002/maco.201206941

[8] Y J Hsu, W C Chiang, J K Wu 2005 *Corrosion behavior of FeCoNiCrCux high-entropy alloys in 3.5% sodium chloride solution* Mater Chem Phys vol 92 p 112–117 doi:10.1016/j.matchemphys.2005.01.001

[9] Y Y Chen, T Duval, U D Hung, J W Yeh, H C Shih 2005 *Microstructure and electrochemical properties of high entropy alloys-a comparison with type-304 stainless steel* Corros. Sci. vol 47 p 2257–2279 doi:10.1016/j.corsci.2004.11.008

[10] P. Huang, J. Yeh 2004 *Multi-Principal Element Alloys with Improved Oxidation and Wear* Resistance for Thermal Spray Coating, Adv. Eng. Mater. 6 74–78. doi:10.1002/adem.200300507

[11] J W Yeh, S K Chen, S J Lin, J Y Gan, T S Chin, T T Shun, C H Tsau, S Y Chang 2004 *Nanostructured high-entropy alloys with multiple principal elements: Novel alloy design concepts and outcomes* Adv. Eng. Mater. vol 6 p 299–303 doi:10.1002/adem.200300567

[12] J Nelson and D Riley 1945 *An experimental investigation of extrapolation methods in the derivation of accurate unit-cell dimensions of crystals* Proc Phys Soc Lond vol 57 p 160 doi: 10.1088/0959-5309/57/3/302

[13] K Y Tsai, M H Tsai, J W Yeh 2013 *Sluggish diffusion in Co-Cr-Fe-Mn-Ni high-entropy alloys Acta Mater vol 61 p 4887–4897 doi:10.1016/j.actamat.2013.04.058*

[14] D B Miracle, O N Senkov 2017 *A critical review of high entropy alloys and related concepts* Acta Mater vol 122 p 448–511 doi:10.1016/j.actamat.2016.08.081

[15] H Oh, D Ma, G Leyson, B Grabowski, E Park, F Körmann, D Raabe 2016 *Lattice Distortions in the FeCoNiCrMn High Entropy Alloy Studied by Theory and Experiment* Entropy vol 18(9) p 321 doi:10.3390/e18090321

[16] Y J Zhou, Y Zhang, F J Wang, G L Chen 2008 *Phase transformation induced by lattice distortion in multiprincipal component CoCrFeNiCuxAl1-x solid-solution alloys* Appl Phys Lett vol 92 241917. doi:10.1063/1.2938690.

[17] F J Wang, Y Zhang, G L Chen 2009 *Atomic packing efficiency and phase transition in a high entropy alloy* J Alloys Compd vol 478 p 321–324 doi:10.1016/j.jallcom.2008.11.059

[18] J Nelson, D Riley 1945 *An experimental investigation of extrapolation methods in the derivation of accurate unit-cell dimensions of crystals* Proc. Phys. Soc. Lond. vol 57 p 160 doi: 10.1088/0959-5309/57/3/302